MARTINI Model for Physisorption of Organic Molecules on Graphite

Gobbo, Cristian; Beurroies, Isabelle; de Ridder, David; Eelkema, Rienk; Marrink, Siewert J.; De Feyter, Steven; van Esch, Jan H.; de Vries, Alex H.

Published in:
Journal of Physical Chemistry C

DOI:
10.1021/jp402615p

Publication date:
2013

THE JOURNAL OF PHYSICAL CHEMISTRY C

Article

pubs.acs.org/JPCC

MARTINI Model for Physisorption of Organic Molecules on Graphite

Cristian Gobbo,[†] Isabelle Beurroies,[‡] David de Ridder,[§] Rienk Eelkema,[†] Siewert J. Marrink,[∥] Steven De Feyter,[⊥] Jan H. van Esch,[†] and Alex H. de Vries*[,∥]

[†]Department of Chemical Engineering, Advanced Soft Matter, Delft University of Technology, Julianalaan 136, 2628 BL Delft, The Netherlands

[‡]Aix Marseille Université, CNRS, UMR 7246, Lab MADIREL, F-13397 Marseille 20, France

[§]Department of Watermanagement, Delft University of Technology, Stevinweg 1, 2628 CN Delft, The Netherlands

[∥]Molecular Dynamics Group, Groningen Biomolecular Sciences and Biotechnology Institute and Zernike Institute for Advanced Materials, University of Groningen, Nijenborgh 7, 9747 AG Groningen, The Netherlands

[⊥]Division of Molecular Imaging and Photonics, Department of Chemistry, KU Leuven-University of Leuven, Celestijnenlaan 200F, B 3001, Leuven, Belgium

ABSTRACT: An extension to the MARTINI coarse-grained model is presented to describe the adsorption of organic molecules on graphite surfaces. The model allows the study of the dynamics of the preferential adsorption of long-chain organic molecules from solvent and the formation of ordered structures on the surface through self-assembly on the microsecond time scale. It was found that the MARTINI model, developed for self-assembling biomolecular systems in solution, could be extended to include two-dimensional self-assembly on a solid surface using a single recipe to determine the interactions of the existing bead-types with the new representation of graphite. The model was parametrized on adsorption enthalpies of small molecules from the gas phase and on wetting enthalpies of pure compounds. Three wetting enthalpies were determined experimentally to extend the range of chemical functionalities parametrized against. The model reproduces order−disorder transitions of hexadecane and hexadecanol and preferential adsorption of long-chain organic compounds from organic solvents, including the formation of lamellar arrangements on the surface.

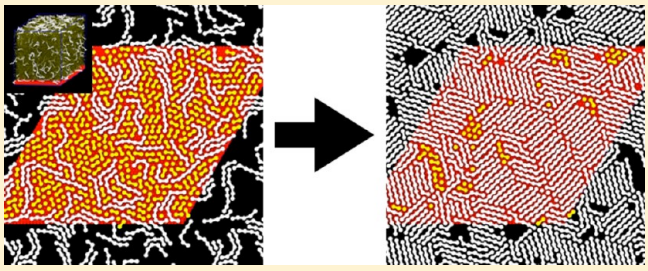

1. INTRODUCTION

Due to the ongoing demand for miniaturization, the design of molecular assemblies in the 0.1−20 nm length range is receiving ample attention.[1−6] Lately, the self-assembly of molecular building blocks has proven itself as a highly promising bottom-up nanopatterning technique, and much progress has been made in this direction.[7−10] The design of such molecular assemblies often relies on qualitative molecular models. Such an intuitive approach does not consider aspects such as the dynamics and conformational freedom of the building blocks in the aggregate and the role of the solvent. Moreover, a better knowledge of the mechanism of formation and reorganization of these aggregates is relevant for gaining a better insight in the phenomena of molecular self-assembly[11−15] and in view of aggregate poststabilization.[16,17] Noteworthy events during the formation and reorganization take place at shorter time scales than those of the commonly used techniques for the study of these aggregates, and therefore only little is known about them. To tackle this issue, molecular dynamics (MD) is proposed for its ability to simulate events on the appropriate time scales. Even though an early united-atom model MD study by Xia and Landman[18] showed preferential adsorption of *n*-hexadecane from an equal weight mixture with *n*-hexane on a Au(001) surface taking place within 1 ns of cooling the mixture down, modeling approaches to date have not explored the spontaneous adsorption further.[19] Fodi and Hentschke showed that reparametrization of standard force fields is likely necessary to obtain reasonable adsorption energies for benzene and *n*-heptane mixtures on graphite.[20] Often, modeling is used to assess the relative energies of proposed alternative surface arrangements, and starts from ordered structures based on scanning tunneling microscopy (STM) pictures, allowing relaxation in short (<1 ns) MD runs.[21,22] A number of studies using MD[23] or Monte Carlo[24] techniques addressed the surface layer structure and diffusion of alkanes, but no study addresses the simulation of the whole process, including adsorption and surface reorganization up to the formation of an ordered monolayer.

The aim of this study is the extension of the well-established MARTINI coarse-grained force field (FF) to develop a design tool for two-dimensional self-assembled nanostructures on graphite, leading to a better understanding of their mechanism of adsorption and reorganization.

Received: March 15, 2013
Revised: July 8, 2013
Published: July 23, 2013

Table 1. Interaction Matrix for MARTINI Beads Used in This Work[a]

bead	C1	C1S	C1E	SG4	SC4	P1	P3
C1	IV	IV	IV	75VI43	V	VI	VII
C1S	IV	III43	V43	75VI43	V	VI	VII
C1E	IV	V43	III43	75VI43	V	VI	VII
SG4	75VI43	75VI43	75VI43	OO24	375V43	75V43	75VI43
SC4	V	V	V	375V43	75IV43	IV	V
P1	VI	VI	VI	75V43	IV	II	II
P3	VII	VII	VII	75VI43	V	II	I

[a]Roman numerals indicate the Lennard–Jones type potential interaction level of the bead–bead interaction as given in the MARTINI model 2.0 (σ = 0.47 nm; ε-values (kJ·mol^{-1}) I: 5.0; II 4.5; III 4.0; IV 3.5; V 3.1; VI 2.7; VII 2.3). Prefixes denote a scaling of the standard C6 and C12 parameters (75 means scale by 0.75, 375 by 0.375). Postfixes denote using a σ other than 0.47 nm (43 means 0.43 nm, 24 0.24 nm). The OO interaction level has ε = 102 kJ·mol^{-1}). C1: alkane bead for short alkanes; C1S: alkane bead for long alkanes in the middle of a chain; C1E: alkane bead for terminal groups of long alkanes; SG4: graphite bead; SC4: benzene/phenyl bead; P1 or P3: alcohol/amide bead.

This work is organized as follows. Section 2 describes the model and the additional measurements of wetting enthalpies of three compounds of interest. Section 3 describes the parametrization strategy and criteria and the tests of the coarse grained (CG) FF on a few archetypical systems. In particular, we show that the model is able to reproduce lamellar assemblies of long-chain alkanes formed by preferentially adsorbing from a solution in short-chain alkanes on graphite, which appear similar to those empirically probed by STM measurements. A discussion of the results is given in Section 4.

2. MODEL AND METHODS

2.1. Interaction Sites. The coarse-grained MARTINI model version 2.0[25] uses a basic 4-to-1 mapping of chemical functional groups to single beads, initially developed to study the physical chemistry of lipid aggregates in water.[26] The beads are classified according to their polarity as major types Q (charged), P (polar), N (neutral), and C (hydrophobic). Version 2.0 introduced aromatic and aliphatic ring compounds, in particular benzene and cholesterol, with a subdivision of the major bead types, to reflect hydrogen-bond donor and/or acceptor capabilities (subtypes 0, d, a, da) and a gradation in polarity (subtypes 1–5). Also, the ring compounds are treated with a basic 2-to-1 mapping, which requires a scaling of the nonbonded interaction levels, and all bead types therefore are extended with a designation "S", to denote the "special" types; for example, three SC4 beads are used to build a benzene molecule.

The present extension of the model introduces new bead types for beads describing the graphite surface and beads describing long-chain organic adsorbent molecules. The graphite layers are represented by hexagonally packed beads of the new type SG4, in a 2-to-1 mapping scheme based on benzene. MARTINI representations of fullerene,[27] carbon nanotubes,[28] and a graphene sheet[29] using a 4-to-1 mapping scheme have been reported. Here, we decided to use a 2-to-1 mapping scheme for graphite because the 4-to-1 scheme requires a bonded network between the beads, whereas the present scheme leaves a multilayered, hexagonally packed graphite model stable by nonbonded interactions only, enabling effortless extension of the layers in all dimensions and thereby allowing the study of very large adsorption areas. Two new bead types are introduced to describe the long-chain organic adsorbent molecules, C1S for alkyl groups in the middle of such chains and C1E for alkyl end groups. They serve to reflect the tendency of longer chains to align on the surface, which reduces the effective size of the coarse-grained beads, and the preference for lamellar structures, in which the termini of the chains are aligned; see Results section.

2.2. Nonbonded Interactions. Nonbonded interactions in the MARTINI force field (FF) are modeled by so-called shift functions. Shift functions cause distance-dependent potentials and forces to smoothly go to zero instead of showing a discontinuity at the cutoff distance. In the MARTINI model, shift functions are applied to modify the Lennard–Jones (LJ) potential and the Coulomb potential.[30] Note that in this work, the Coulomb potential is not used because there are no beads that carry a charge. The shifted LJ potential is given by eq 1:

$$\Phi(r) = \begin{cases} 4\varepsilon\left(\sigma^{12}\left[\frac{1}{r^{12}} - S_{12}\right] - \sigma^{6}\left[\frac{1}{r^{6}} - S_{6}\right]\right); & r \le r_c \\ 0; & r > r_c \end{cases} \tag{1}$$

with:

$$S_n = \frac{nA_n}{3}(r - r_s)^3 + \frac{nB_n}{4}(r - r_s)^4 + \frac{1}{r_c^n} + \frac{nA_n}{3}(r_c - r_s)^3 + \frac{nB_n}{4}(r_c - r_s)^4 \tag{2}$$

and:

$$A_n = -\frac{(n+4)r_c - (n+1)r_s}{r_c^{n+2}(r_c - r_s)^2};$$
$$B_n = -\frac{(n+3)r_c - (n+1)r_s}{r_c^{n+2}(r_c - r_s)^3} \tag{3}$$

Here, r_c is the cutoff and r_s the distance from which the shifting takes effect. For the LJ interaction in the MARTINI model, r_c = 1.2 nm and r_s = 0.9 nm. The two parameters that determine the LJ interaction are related to the depth of the potential energy well (ε) and the effective size of the beads (σ). To prevent a proliferation of parameters, the original MARTINI model uses a single value σ = 0.47 nm for all beads; version 2.0 introduces the special beads which are smaller, σ = 0.43 nm to reflect the 2-to-1 mapping. In MARTINI version 2.0, the interaction strengths are limited to 10 distinct levels, labeled O to IX with decreasing values of ε from 5.6 to 2.0 kJ·mol^{-1}. The parametrization of the interaction levels is based on partitioning free energies of functional chemical groups, represented by small molecules, mapping to the defined bead types, for example, butane to C1, propanol to P1, and methylformamide to P3. An interaction matrix then

dx.doi.org/10.1021/jp402615p | J. Phys. Chem. C 2013, 117, 15623–15631

Table 2. Bonded Interactions for Molecules Used in This Work[a]

bond	$V(r) = 1/2K_b(r - r_0)^2$		angle	$V(\theta) = 1/2K_a(\cos\theta - \cos\theta_0)^2$	
beads	r_0 (nm)	K_b (kJ·mol^{-1}·nm^{-2})	beads	θ_0 (deg)	K_a (kJ·mol^{-1})
C1X-C1X	0.51	1250	C1X-C1X-C1X	180	30
Pol-C1X	0.51	1250	C1X-Pol-C1X	180	30
			Pol-C1X-C1X	180	30
C1-C1	0.51	1250	C1-C1-SC4	180	25
C1-SC4	0.37	2500	C1-SC4-SC4	150	50
SC4-SC4	0.27	constraint			

[a]C1X = C1S or C1E, Pol is the polar bead (P1 or P3) representing bead containing an alcohol or amide functional group. SC4 is a benzene/phenyl bead.

defines the LJ parameters for all the (cross) interactions between bead types in terms of the interaction levels. The special bead types interact with normal bead types in the same manner as normal bead types, but for special bead types interacting with other special bead types, the ε-values are scaled by 75% because of the increased energy density as a consequence of the smaller size of the special bead types.

In the present extension, parametrization was performed on enthalpies because most relevant experimental data report enthalpies only. The first round of parametrization used adsorption enthalpies of individual molecules on the surface, see the Results section. Subsequent rounds used wetting enthalpies of pure liquids on graphite and displacement enthalpies of solutes (long-chain organic molecules) from different solvents (heptane and phenyloctane). The final interaction table for the beads used in this work is given in Table 1.

2.3. Bonded Interactions. The LJ interaction between nearest-neighbor beads is excluded; instead, they interact via harmonic bonds, eq 4:

$$V_b(r) = \frac{K_b}{2}(r - r_0)^2 \quad (4)$$

Here, K_b is the force constant for the bond-stretching potential, and r_0 is the distance at which the potential is zero. Angle potentials may also be added between neighboring bonds, eq 5:

$$V_a(\theta) = \frac{K_a}{2}(\cos\theta - \cos\theta_0)^2 \quad (5)$$

Here, K_a is the force constant and θ_0 is the angle at which the potential is zero. Standard bond-stretching parameters for alkanes are r_0 = 0.47 nm and K_b = 1250 kJ·mol^{-1}·nm^{-2}; standard angle-bending parameters for alkanes are θ_0 = 180° and K_a = 25 kJ·mol^{-1}. These values are optimized to reproduce the properties of alkanes in isotropic fluids and solutions. Long-chain alkanes and organic molecules adsorbed on the graphite surface adopt more stretched conformations, which is reflected in this extension by somewhat longer bonds and stiffer angles. The bonded parameters for the model are given in Table 2.

2.4. Simulation Setup and Details. All simulations were run with the GROMACS simulation package, version 4.[31] The equations of motion were integrated numerically with a time-step of 30 fs. A triclinic unit cell (simulation box) was used, with the lateral dimensions fixed, so that the basal plane is commensurate with a hexagonal lattice of the graphite beads. The perpendicular dimension was kept orthogonal to the basal plane, but not fixed in length. Periodic boundary conditions were applied in all directions, so that each unit cell has two solid−liquid interfaces. A five-layer thick surface was built so that adsorption from solution could take place without direct interaction between molecules adsorbed on opposite sides of the graphite surface layer (their distance is approximately 1.6 nm, well outside the cutoff range of the potential, 1.2 nm). Pressure coupling to a pressure of 1.0 bar was achieved through the Berendsen barostat[32] with a coupling time of 3.0 ps and a compressibility in the z-direction of 3×10^{-5} bar^{-1}. The temperature was maintained by coupling to a bath through a Berendsen thermostat[32] with a coupling constant of 0.3 ps. Long-chain adsorbents and solvent were coupled to separate temperature coupling baths. The graphite beads were always frozen. Thus, there is no dynamics in the beads making up the surface. Most systems consisted of 18 000 graphite beads, spanning a hexagonal basal plane with dimensions of 16.2 × 14.02 nm^2. Depending on the number of adsorbent and solvent molecules, and temperature the unit cell had a height (z-dimension) of 6−12 nm. The simulation times were in the microsecond range. Here, we report unscaled simulation times. In general, in CG models, dynamical processes occur faster than in corresponding all-atom simulations because of the reduced friction due to the smoother potentials. In principle, the correspondence to real time within each model should be gauged against experiment or all-atom simulations.[33] For the MARTINI model, a speed-up of about a factor of 4 was found in liquid systems and lipid bilayers based on diffusion of solvent and lipids.[26]

2.5. Analysis. Adsorption enthalpies of single molecules from the gas phase were calculated by subtracting the average potential energy of a single adsorbent molecule in vacuo from that of a system containing the graphite surface and a single adsorbent molecule and subtracting RT (2.5 kJ·mol^{-1}) to account for the change from the gas phase to condensed phase for the adsorbent molecule. Note that, because the graphite surface is treated as frozen, it does not contribute to the energy. Wetting enthalpies were calculated by subtracting the average potential energy of a system containing only adsorbent molecules (a melt) from the average energy of a system containing the same number of adsorbent molecules and the graphite surface, and dividing by the total graphite surface area (454.25 nm^2, accounting for two interfaces in the unit cell). Displacement enthalpies, that is, the heat liberated when a surface saturated with solvent is eluted with a different solution, were calculated by subtracting the wetting enthalpy of pure solvent from the wetting enthalpy of the solution.

Mass density profiles across the system were calculated with the GROMACS tool g_density, converting from the standard MARTINI bead masses to the real masses of the fragments represented by the beads.

2.6. Measurement of Wetting Enthalpies. Wetting enthalpies (mJ·m^{-2}) were obtained dividing the heat of

dx.doi.org/10.1021/jp402615p | J. Phys. Chem. C 2013, 117, 15623−15631

immersion by the graphon (i.e., carbon in the form of graphite) surface area, using an isothermal Tian-Calvet type microcalorimeter[34] that is described in Denoyel et al.[35] A glass ampule with a brittle end was filled with graphon (0.2−0.3 g). The ampule was placed in "the clarinette", and the regular vacuum was applied. When a pressure of 2×10^{-1} mbar was reached, the regular vacuum was closed, and high vacuum was engaged, reaching a pressure of 1×10^{-2} mbar. The sample was heated at 105 °C, with a temperature increase of 10 °C/min. The sample was cooled down to ambient temperature. The ampule (still under vacuum) was sealed and ready for analysis. Next, the calorimetric cell was filled with 7 mL of liquid. For 1-hexadecanol and *N*-butyldodecanamide (N-BDDA), this corresponds to 4.996 and 5.405 g, respectively. This was added as dry mass to the calorimetric cell and, if necessary, compressed. The calorimetric cell was heated until the material was liquefied, and then the ampule and push rod assembly was quickly connected to the cell, and the whole assembly was placed in the calorimeter. The calorimeter was set at a given temperature and amplifier voltage. After placement of the ampule, push rod, and cell, the calorimeter has to reach thermal equilibrium again before analysis, which typically takes 5−6 h. Next, the ampule was broken and the released heat recorded until thermal equilibrium was reached again (which typically takes 1−2 h), and corrected for the heat released by breaking the ampule. The wetting enthalpy per unit of surface area is calculated from the measured heat and the surface area of the graphon.

The surface area of the graphon was determined from the adsorption isotherm of N_2. The relevant part of the adsorption isotherm of N_2 on graphon was recorded at 77 K on a Micromeritics TriStar 3000 adsorption analyzer. The graphon sample was degassed in vacuum (1×10^{-2} mbar) for 12 h at 105 °C and then cooled to liquid nitrogen temperature (77 K). Portions of nitrogen were dosed into the sample cell. The multipoint BET specific surface area (S_{BET}) was determined according to the BET (Brunauer, Emmett, and Teller) theory[36] from the measurements in the pressure range between 0.05 and 0.25 mbar.

3. RESULTS

3.1. Parametrization of the Graphite Surface. Graphite beads, named SG4, were modeled analogously to the benzene beads (SC4) in the MARTINI model version 2.0. The interaction between SG4 beads should be stronger than those between SC4 beads because the surface beads are supposed to pack with the density appropriate for graphite. Assuming hexagonal packing, this means a bead−bead distance of 0.27 nm. This may be achieved by using a modified σ of 0.24 nm and a very strong interaction ε = 102 kJ·mol^{-1}. Using those parameters, the beads when started off on a hexagonal lattice of correct dimensions largely remain on that lattice, but over time defects do occur, and the simulations are stable only with a relatively short time step. Therefore, in all other simulations, the graphite surface was treated as a static surface, the beads not taking part in the dynamics. The surface beads should provide both the energy density appropriate to yield the correct adsorption enthalpy for individual molecules and the orientational biasing of lamellar—or other—structures.

3.2. Parametrization of Adsorbent Molecules. Initial FF parametrization of the nonbonded interactions for adsorption on graphite targeted adsorption enthalpies from the gas phase for individual molecules as far as these are known.[37,38] Initially, the SG4−other bead interactions were set the same as those between benzene (SC4) beads and other beads, but this yielded adsorption enthalpies that were approximately a factor of 2 too strong compared to experimental values (data not shown), owing to the higher energy density in the hexagonal packing of the surface beads compared to ring structure of benzene. Scaling down the ε-values by a factor of 2 for the SC4−SG4 interaction and using the special type interaction also for nonring particles improved the agreement with experiment (data not shown). The rationale for the choice to use the interaction between special bead types also for normal beads in interaction with the surface is that the adsorption process leads to a condensation of the adsorbents and the distance between alkyl chain and surface is smaller than between alkyl chains in the melt. Using the special bead type interactions for adsorbent−surface interactions, the adsorbents have a smaller size with respect to the surface. In a final refinement all interactions were made one level weaker, leading to the adsorption enthalpies of single molecules shown in Column 3 of Table 3. It should be noted that the above rules constitute a simple and straightforward recipe to convert molecules from the standard MARTINI model to the present model suitable for the study of adsorption on a graphite surface, in keeping with the MARTINI model's maxim of simplicity. Given the semiquantitative nature of the MARTINI model and the limited range of pertinent experimental data, quantitative results for individual adsorbents are not expected, nor the object of the model. The interaction matrix for the beads used in this study is given in Table 1.

More important for the intended use of the model is the behavior of the longer-chain molecules at the wetting limit or on being adsorbed from mixtures. Preferential adsorption of long-chained alkanes (6 beads) from short-chain alkanes (2

Table 3. Adsorption and Wetting Enthalpies of Selected Molecules onto Graphite[a]

		$-\Delta H_{ads}$ (kJ·mol^{-1})		$-\Delta H_w$ (mJ·m^{-2})	
molecule	representation	model	exp.	model	exp.
butane	C1	27	54[37,b]	n.d.	n.d.
octane	C1-C1	51	54[37,b]	194	122[39,d]
hexadecane	C1E-C1S-C1S-C1E	108	114[c]	214[d]	200[46,e]
do/tetracosane	C1E-(C1S)$_4$-C1E	151	150[c]	n.d.	n.d.
benzene	-SC4-SC4-SC4-(ring)	41	44[37]	93	111[39]
phenyloctane	C1-C1-SC4-SC4-SC4- (ring)	91	n.d.	140	59
butanol	P1	31	60[38]	n.d.	n.d.
octanol	P1-C1	55	84[c]	196	175[40]
decanol	P1-C1E	55	84[c]	218	n.d.
hexadecanol	P1-C1S-C1S-C1E	111	132[c]	203	175,[46] 150[f]
tetracosanol	P1-(C1S)$_4$-C1E	163	180[c]	n.d.	n.d.
N-BDDA	C1E-P1-C1S-C1E	111	n.d.	195	131[f]

[a]All values at 298 K, unless otherwise noted. In the model, the adsorption enthalpy was calculated as the difference in energy between the adsorbent(s) with and without surface present, and subtracting RT (= pV) to account for the condensation onto the surface. Experimental data for the adsorption and wetting enthalpies are in some cases based on extrapolations. [b]Value for hexane. [c]Based on an additive contribution of 6.0 kJ·mol^{-1} per CH_2 group. [d]Value for heptane. [e]At 338 K. [f]At 358 K.

dx.doi.org/10.1021/jp402615p | J. Phys. Chem. C 2013, 117, 15623−15631

beads), representing the experimentally characterized docosane ($C_{22}H_{46}$) adsorbent from heptane (C_7H_{16}) solvent,[39] was observed with the model parametrized on the basis of the gas-phase adsorption enthalpies. The displacement enthalpy, that is, the heat liberated when a surface saturated with solvent is eluted with a different solution, was, however, not large (and negative) enough compared to experimental data, and the structures formed on the surface, although showing a tendency to form lamellar arrangements, were not very stable (data not shown). Therefore, the final round in the parametrization focused on reproducing the collective effects in adsorption, both in wetting and as seen in preferential adsorption of long-chain alkanes, alcohols, and amides from shorter-chain alkane or phenyloctane solutions. Here, the objective was to reproduce to a reasonable extent the wetting enthalpy, the displacement enthalpy, the formation of lamellar surface structures observed by STM, and the area the adsorbed molecules occupy on the surface.

Wetting and displacement enthalpies were largely taken from the literature,[40] but the wetting enthalpies of a number of compounds were also measured to have more targets for parametrization. In particular, the use of the same polar bead type for the alcohol and amide groups that appears natural because both groups are of H-bond donor−acceptor type may not be warranted. The wetting enthalpies of 1-hexadecanol, *N*-butyldodecanamide (N-BDDA), and phenyloctane were determined with immersion calorimetry; see Section 2.6. The experimental measured heats and their final conversion to $mJ·m^{-2}$ based on a graphon surface area of 216 $m^2·g^{-1}$ are reported in Table 4.

Table 4. Wetting Enthalpies of Selected Molecules onto Graphite[a]

	1-hexadecanol (85 °C, 3 mV)	N-BDDA (85 °C, 3 mV)	1-phenyloctane (25 °C, 1 mV)
measured heat (mJ)	8758.932	4397.225	3621.220
mass graphon (g)	0.2876	0.1557	0.2852
heat of immersion ($mJ·g^{-1}$)	30455.26	28241.65	12697.12
wetting enthalpy ($mJ·m^{-2}$)	150.00	130.75	58.78

[a]Data for determination of wetting enthalpy. The wetting enthalpy is calculated from the measured heat and the mass of graphon, using the specific surface area of graphon of 216 $m^2·g^{-1}$ determined from the BET isotherm of nitrogen.

Calculated wetting enthalpies for a number of adsorbents are given in Column 5 of Table 3. Given the coarse-grained nature of the model, quantitative agreement is not expected because the same coarse-grained molecule represents several possible real molecules and the thermodynamic and structural properties depend on the length of adsorbents and solvents. The semiquantitative nature of the MARTINI model is, however, preserved. To mimic the collectivity of the adsorption and to favor longer-chain alkanes on the surface over short-chain alkanes, (1) we strengthened the lateral interactions between the chains by giving only the long-chain alkane beads a reduced size when interacting with each other (C1S beads, see Table 1) and (2) favored straightened chains by increasing the bond lengths from the standard 0.47 to 0.51 nm, as well as (3) using a higher force constant on the angle bending potential (30 instead of the standard value of 25 $kJ·mol^{-1}$, see Table 2) and (4) introducing long-chain alkane terminal beads (C1E beads, see Table 1) which interact with each other more strongly than with other alkane beads. Care needs to be taken in applying these changes. First of all, reducing the size too much leads to strong aggregation of the long chains in solution. Although segregation of differently sized alkanes in mixtures is observed under some conditions,[41−43] it was deemed undesirable in the model. Also, too-small bead sizes lead to too-small areas per molecule once adsorbed on the surface and to the formation of a second layer of adsorbent, which is not observed experimentally.[44] The final model leads to a surface area per molecule of alkanes of length 22−26 C-atoms (the range spanned by 6 beads) of 1.13−1.34 nm^2. We also found that surface mobility was reduced when increasing the bond length to yield correct areas per molecule. Strongly reduced surface mobility basically prevents the system from rearranging to thermodynamically more favorable arrangements due to kinetic barriers. We therefore settled for a compromise between the area per molecule, displacement enthalpy, and surface mobility. The final nonbonded and bonded parameters are described in Tables 1 and 2, respectively. Note that the changes in parameters describing long-chain alkanes affect the properties of pure long-chain alkane melts. For example, the density of hexadecane calculated as 860 $kg·m^{-3}$ at 298 K is somewhat higher than the value of 832 $kg·m^{-3}$ in the standard MARTINI model. Since the interaction between long-chain alkane beads and normal solvent beads is not changed, solvation free energies of long-chain alkanes at low concentrations are not affected. At higher concentrations, mixing and partitioning properties are expected to show changes compared to the standard MARTINI model. We have not investigated changes in solution properties in detail, other than those mentioned already. The focus of the present model is the behavior of the long-chain molecules on the graphite surface. More detailed results showing the collective behavior of adsorbents on graphite are given in the next two sections.

3.3. Order−Disorder Transition of Linear Alkanes and Primary Alcohols. Pure hexadecane and pure hexadecanol have been shown to undergo an order−disorder transition on a graphite surface, as evidenced by a decrease in excess surface mass as a function of temperature.[40,45,46] The behavior of the excess surface mass is similar for hexadecanol and hexadecane when plotted against $T-T_m$, where T_m is the temperature at which the pure compound melts. The excess surface mass is (approximately) related to the adsorption enthalpy and yields similar values for hexadecane and hexadecanol. The present model shows a clear transition from multilamellar structures adsorbed on the surface to a disordered phase between 358 and 368 K for pure hexadecanol on graphite. Snapshots of the two systems at different temperatures are shown in Figure 1. The wetting enthalpy drops from ∼300 $mJ·m^{-2}$ in the ordered phase to ∼210 $mJ·m^{-2}$ in the disordered phase. This drop is reasonably close to the experimental estimation[39] of ∼75 $mJ·m^{-2}$, and the absolute values are also reasonable; see Table 3. A similar drop in wetting enthalpies is observed for hexadecane between 328 and 338 K; however, this transition is much less clear in terms of the structure because the system freezes in a glassy state. Both transition temperatures are in very good agreement with experiment, which places the transition 30−40 K above the melting temperature in both cases (the experimental melting temperatures of hexadecanol and hexadecane are 322 K and 291 K, respectively).

dx.doi.org/10.1021/jp402615p | J. Phys. Chem. C 2013, 117, 15623−15631

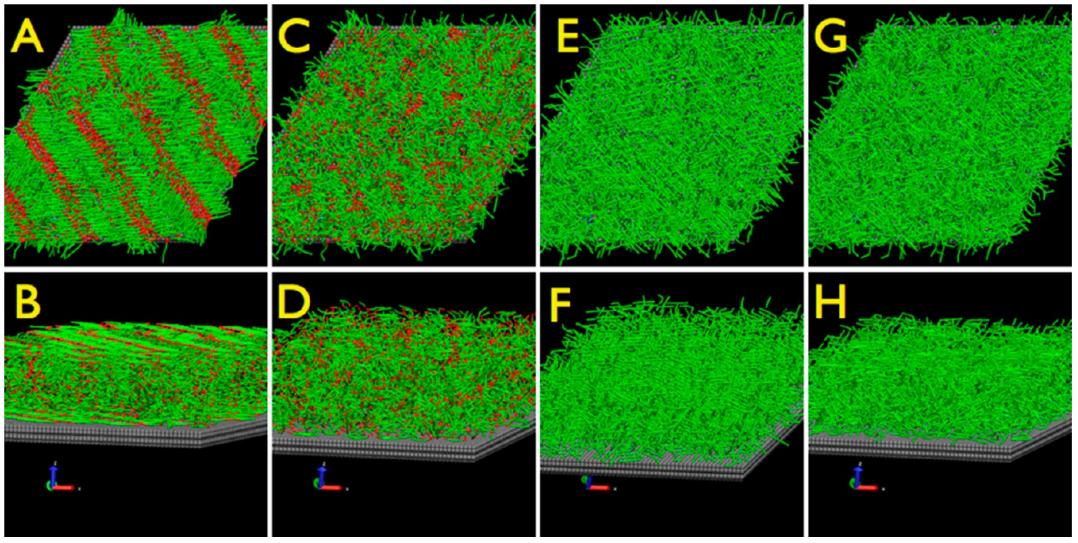

Figure 1. Order−disorder transitions in pure hexadecanol and hexadecane on a graphite surface. Snapshots of hexadecanol at 358 K (A, B) and 368 K (C, D). Snapshots of hexadecane at 328 K (E, F) and 338 K (G,H). Graphite beads are shown as gray van der Waals spheres. Hexadecanol and hexadecane are shown in licorice representation. Alkyl C-type beads are colored green; alcohol P-type beads are colored red. Pictures are made with VMD.[48] Note that the molecules at the top of the pictures are adsorbed on graphite too; that is, the molecules are sandwiched between two graphite substrates, due to the periodic boundary conditions. The graphite substrate on top is not shown.

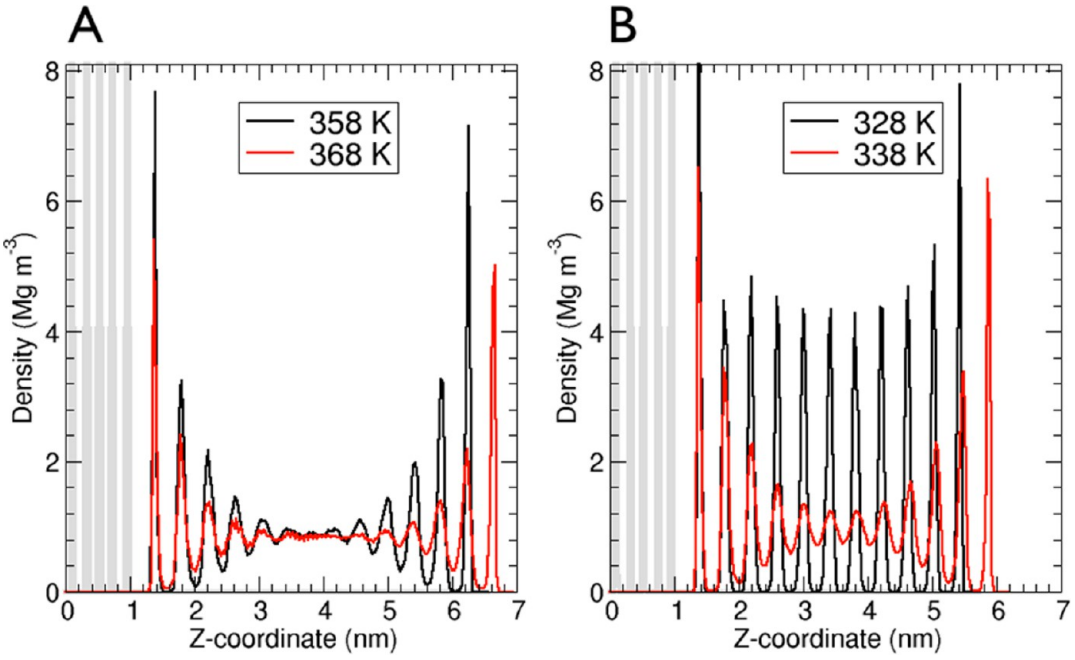

Figure 2. Mass density profile across the system perpendicular to the surface for pure hexadecanol (A) and hexadecane (B) on graphite surface below (black) and above (red) the order−disorder transition. The density of the graphite sheets, shown as thick gray lines, spikes to higher values, outside the range of the plot. Note that another five layers of graphite of which the density is not shown are present at the right-hand side of the graphs, adjacent to the rightmost peak of each system.

Density profiles along the direction perpendicular to the surface, shown in Figure 2, also demonstrate the order−disorder transition of pure hexadecanol and hexadecane on graphite. In the low-temperature, ordered structures, both hexadecanol and hexadecane molecules form clear layers visible in the density profile, starting on the surface and persisting for several layers. Above the transition, the order clearly decreases a few layers away from the surface. In addition, hexadecanol shows clear lamellar structure below the transition, persisting also into several layers away from the surface, as seen in Figure 1A. In terms of layering, hexadecane appears to be more structured than hexadecanol. The closer packing is likely due to the lower temperatures for the hexadecane system. The tendency to form lamellar arrangements is clearly less strong for hexadecane than for hexadecanol.

3.4. Preferential Adsorption. Mixtures of long-chain and short-chain alkanes over a graphite surface show preferential adsorption of the long-chain alkanes. The present model reproduces this behavior. Starting from a solution of a 6-bead alkane from a 2-bead alkane (representing the experimentally characterized docosane-heptane mixture[39]), the longer-chain alkane is seen to preferentially adsorb on the surface. Snapshots

dx.doi.org/10.1021/jp402615p | J. Phys. Chem. C 2013, 117, 15623−15631

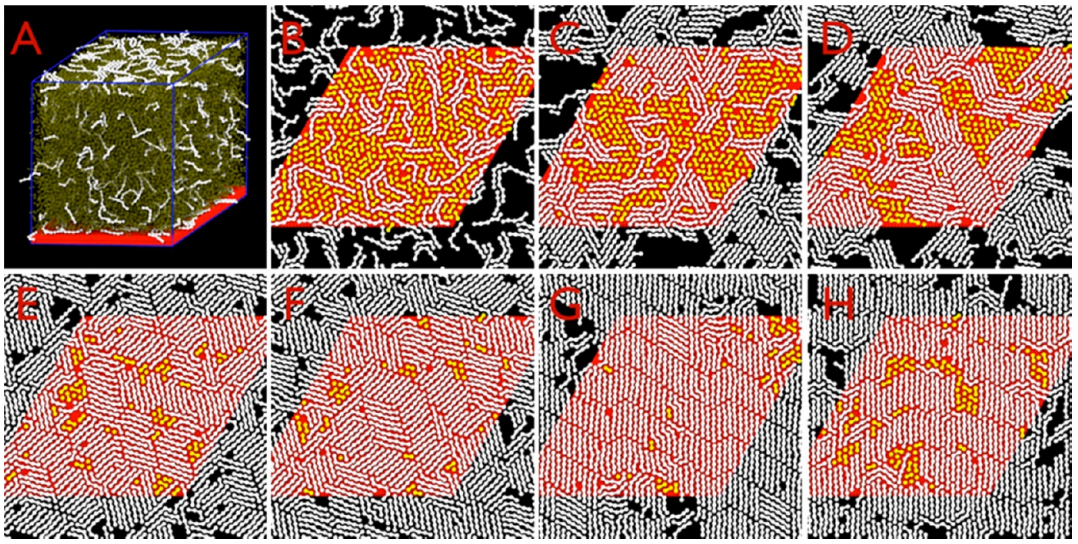

Figure 3. Preferential adsorption and reorganization of long-chain alkanes from short-chain alkanes on graphite. Starting from a random solution (A, 0 ns), long-chain alkane is seen to adsorb preferentially on the graphite surface (B, 100 ns). Adsorbed long-chain alkanes tend to cluster (C, 200 ns), but the clusters and the lamellar ordering within the clusters are not stable (D, 300 ns). The surface becomes almost exclusively covered by long-chain alkanes (E, 600 ns), with a slowing down of the reorganization dynamics, leaving multiple lamellar domains (F, 1000 ns) that show limited rearrangement on the time scale of hundreds of nanoseconds. Although the lamellar state of the adsorbed long-chain alkanes is preferred, a long-time simulation starting from a well-ordered lamellar state (G, 0 ns) shows that rearrangements, (partial) desorption, and adsorption take place on the microsecond time scale (H, 6000 ns). Long-chain alkanes are shown in a white ball-and-stick model. Solvent is shown in a yellow stick representation (B–H) or transparent dark green (A), and the graphite surface beads are shown as red van der Waals spheres. In A, the unit cell boundaries are shown as blue lines. Note that the molecules at the top of the picture in A are adsorbed on graphite, which is not shown. In B–H only the lower surface is shown and only the beads that are adsorbed to the surface, which may lead to showing truncated molecules—the other beads then stick up from the surface into the solution. In B–H, periodic images are displayed only for the long-chain alkane to better show their assembly.

of the adsorption process are shown in Figure 3 and demonstrate that long-chain alkane molecules, once diffused to the surface, tend to remain on the surface and through their favorable lateral interactions with other long-chain alkanes compete successfully with short-chain alkane for surface coverage. On the surface, the long-chain alkanes tend to form lamellar aggregates that become more stable once the surface contains more long-chain alkane molecules. The time scale on which stable lamellae, such as seen in STM images with persistence lengths of >10 nm, are formed is considerably larger than 2 μs in this model. The adsorbent molecules form smaller aggregates that randomly adopt one of three orientations on the surface (Figure 3F), reflecting the underlying hexagonal arrangement of the graphite beads. In this model, adsorption to the surface is faster than reorganization of the small aggregates on the surface leading to a nearly fully covered surface covered by relatively small lamellar domains. We also started a simulation from a well-ordered lamellar system of long-chain molecules (Figure 3G) and established that, when enough of such molecules are present in the system, the surface will be nearly fully covered with the long-chain molecules on long time scales but that some disorder remains (Figure 3H); that is, the system is dynamic enough that occasionally long-chain molecules desorb leading to defects in the multilamellar structure.

4. DISCUSSION AND CONCLUSION

Coarse-grained molecular dynamics models, such as the MARTINI model, are powerful tools to study processes at time and length scales at near-atomistic level, where they are currently inaccessible by fully atomistic models. The application of the MARTINI model to date has focused on biomolecular systems in solution, such as the rich aggregation behavior of lipids in water and the interaction between proteins. The attraction of the MARTINI model is its definition in terms of chemical functional groups, inviting extensions to broader areas of application. In this work, the adsorption of organic molecules on graphite is the subject of study.

In defining the beads representing graphite, the choice to use a 2-to-1 mapping was based on the MARTINI model for benzene. A 2-to-1 mapping preserves the hexagonal lattice underlying three equivalent directions on which lamellar arrangements can be formed. The advantage over the 4-to-1 mappings published in the literature for carbon nanotubes and graphene is that a solid surface can be easily built and extended indefinitely without the need to specify bonded interactions. The energy density of the 2-to-1 mapped surface is high and requires reparameterization of the interactions between the surface beads and adsorbent species. Parameterization of the standard MARTINI model uses free energies of partitioning between different solvents. Such thermodynamic data are scarce for adsorption; enthalpic data are more abundant. Therefore, adsorption enthalpies of single molecules from the gas phase were used as input, together with wetting enthalpies.

Adsorption enthalpies were reproducible to semiquantitative level with a single recipe, taking the interaction matrix of version 2.0 of the MARTINI model. It may be noted that, at the coarse-grained level, the adsorption enthalpies of single molecules are bead-additive. To the extent this is measurable; this is also seen experimentally.[38] For longer-chain alkanes, the agreement of the model with the experiment is excellent. For alcohols, the difference with the experiment appears to be larger than necessary for the adsorption enthalpy of single molecules. Note, however, that the experimental data are available only for alcohols up to *n*-butanol, and extrapolated values were used.

dx.doi.org/10.1021/jp402615p | J. Phys. Chem. C 2013, 117, 15623–15631

Important for the intended use of the model is the formation of ordered structures on the surface and the preferential adsorption from mixtures. The model reproduces these for longer chains from solvents. Thus order−disorder transitions of hexadecanol and hexadecane occur at roughly the correct temperature, and docosane adsorbs preferentially from heptane, forming lamellar arrangements on the surface akin to those observed experimentally. Note that the energy gained from interaction of the single beads with the surface does not depend on the alkane. Packing longer-chain alkanes on the surface, however, more beads fit on the surface lowering the total energy. The most important gain, however, is due to the lateral interaction energy, modeled here by using smaller beads for the long-chain alkanes. It should be noted that some fine-tuning of the model to enhance these effects was required. The lamellae can be made more stable by increasing the lateral interaction and/or increasing the bond lengths and stiffness of the angles. However, changing the interactions in this manner had to be done with care because larger changes than described in the final model lead to a number of probably less realistic behaviors. (1) Structures freeze in; that is, starting from solution structures, the multidomain pattern that is formed becomes frozen in, and no rearrangements are seen over many microseconds of simulation. (2) Multiple layers of adsorbent are formed on the surface. (3) Adsorbent molecules strongly aggregate in solution. The difficulties encountered here are reminiscent of the modeling of the gel phase of phospholipids[47] and illustrate the limitations of the MARTINI model in particular and coarse-grained models in general, in which the balance between enthalpic and entropic contributions is shifted with respect to more detailed models.[30] The size of the beads reflects the thermal motions of a number of atoms in a particular state or phase. The MARTINI model was developed for liquid (crystalline) phases and can, to some extent, model other phases as well. The gel state found for phospholipids does not show the correct ordering and tilt of the alkyl tails because the effective size of the beads and the bond length of the stretched chain as found in the gel state do not match the standard values of the model. A similar change in packing is an important driving force in the adsorption and stabilization of long-chain alkanes on graphite. The reduction in motional freedom must be accounted for explicitly in the parameters to fully reflect these changes. Thus, the present extension of the model is biased toward reproducing the properties of the adsorbents on the surface over those in solution.

Long-chain alkanes, alcohols, and amides adsorb preferentially from short-chain alkane and phenyloctane solutions at 298 K, and extensive analysis of these systems is presented elsewhere. Preferential adsorption of long-chain alkanes from octane is decidedly less strong, probably because the wetting enthalpies of octane and long-chain alkane are not sufficiently different. It has been found experimentally[39] that the displacement enthalpy approximately equals the difference in wetting enthalpies between solvent and solute at a solute concentration that is high enough to have full surface coverage by the solute. The displacement enthalpy at full surface coverage for 6-bead alkane from 2-bead alkane was found to be 21 $mJ{\cdot}m^{-2}$ in this model, where the experimental value is 72 $mJ{\cdot}m^{-2}$. For all 6-bead molecules investigated in this study, the displacement enthalpy from phenyloctane was ∼60 $mJ{\cdot}m^{-2}$. To our knowledge, for these systems, experimental values are not available; they are highly desirable as targets for a more quantitative model. Comparing the wetting enthalpies of hexadecanol between the result of Findenegg (Table 3) and our own measurements (Table 4), it is seen that the parametrization may suffer from having to use data from different sources. It is clear, however, that although the wetting is quantitatively too strong, differences in wetting enthalpies are well-reproduced. Preferential adsorption of hexadecanol and N-BDDA from phenyloctane is predicted to be too weak, judging from a comparison of our own data. The model could possibly be improved quantitatively by lowering the wetting enthalpies of phenyloctane and octane at the expense of the adsorption enthalpy from the gas phase, but since this would only result in and even stronger preferential adsorption of the long-chain adsorbents, qualitative changes are not expected.

In conclusion, the model reproduces semiquantitatively adsorption and displacement enthalpies of long-chain organic molecules, enabling the study of a range of processes at molecular resolution. We hope to address a number of interesting questions concerning mechanism and dynamics of adsorption on surfaces, including the formation of nanoscale patterns by self-assembly with the vista to rationally design molecules and test them computationally before embarking on their expensive and time-consuming synthesis.

AUTHOR INFORMATION

Corresponding Author

*Tel: +31503634336; e-mail: A.H.de.Vries@rug.nl.

Notes

The authors declare no competing financial interest.

ACKNOWLEDGMENTS

This work is supported by a NWO VICI grant, The Netherlands. C.G. thanks ERA Chemistry/NWO grant.

REFERENCES

(1) Feldkamp, U.; Niemeyer, C. M. Rational Design of DNA Nanoarchitectures. *Angew. Chem., Int. Ed.* **2006**, *45*, 1856−1876.

(2) Feng, X.; Jiang, L. Design and Creation of Superwetting/Antiwetting Surfaces. *Adv. Mater.* **2006**, *18*, 3063−3078.

(3) Mishra, A.; Ma, C.-Q.; Baeuerle, P. Functional Oligothiophenes: Molecular Design for Multidimensional Nanoarchitectures and Their Applications. *Chem. Rev.* **2009**, *109*, 1141−1276.

(4) Nie, Z.; Li, W.; Seo, M.; Xu, S.; Kumacheva, E. Janus and Ternary Particles Generated by Microfluidic Synthesis: Design, Synthesis, and Self-Assembly. *J. Am. Chem. Soc.* **2006**, *128*, 9408−9412.

(5) Ulijn, R. V.; Smith, A. M. Designing Peptide Based Nanomaterials. *Chem. Soc. Rev.* **2008**, *37*, 664−675.

(6) Rothemund, P. W. K. Folding DNA to Create Nanoscale Shapes and Patterns. *Nature* **2006**, *440*, 297−302.

(7) Lewis, P. A.; Donhauser, Z. J.; Mantooth, B. A.; Smith, R. K.; Bumm, L. A.; Kelly, K. F.; Weiss, P. S. Control and Placement of Molecules via Self-Assembly. *Nanotechnology* **2001**, *12*, 231−237.

(8) Elemans, J.; Lei, S. B.; De Feyter, S. Molecular and Supramolecular Networks on Surfaces: From Two-Dimensional Crystal Engineering to Reactivity. *Angew. Chem., Int. Ed.* **2009**, *48*, 7298−7332.

(9) Kudernac, T.; Lei, S. B.; Elemans, J.; De Feyter, S. Two-Dimensional Supramolecular Self-Assembly: Nanoporous Networks on Surfaces. *Chem. Soc. Rev.* **2009**, *38*, 402−421.

(10) Palma, C. A.; Bonini, M.; Breiner, T.; Samori, P. Supramolecular Crystal Engineering at the Solid-Liquid interface from First Principles: Toward Unraveling the Thermodynamics of 2D Self-Assembly. *Adv. Mater.* **2009**, *21*, 1383−1386.

(11) Rabe, J. P.; Buchholz, S. Direct Observation of Molecular-Structure and Dynamics at the Interface between a Solid Wall and an

Organic Solution by Scanning Tunneling Microscopy. *Phys. Rev. Lett.* **1991**, *66*, 2096−2099.
(12) Buchholz, S.; Rabe, J. P. Molecular Imaging of Alkanol Monolayers on Graphite. *Angew. Chem., Int. Ed.* **1992**, *31*, 189−191.
(13) Samori, P.; Mullen, K.; Rabe, H. P. Molecular-Scale Tracking of the Self-Healing of Polycrystalline Monolayers at the Solid-Liquid Interface. *Adv. Mater.* **2004**, *16*, 1761−1765.
(14) Lackinger, M.; Griessl, S.; Kampschulte, L.; Jamitzky, F.; Heckl, W. M. Dynamics of Grain Boundaries in Two-Dimensional Hydrogen-Bonded Molecular Networks. *Small* **2005**, *1*, 532−539.
(15) De Feyter, S.; Xu, H.; Mali, K. Dynamics in Self-assembled Organic Monolayers at the Liquid/Solid Interface Revealed by Scanning Tunneling Microscopy. *Chimia* **2012**, *66*, 38−43.
(16) Lafferentz, L.; Eberhardt, V.; Dri, C.; Africh, C.; Comelli, G.; Esch, F.; Hecht, S.; Grill, L. Controlling on-Surface Polymerization by Hierarchical and Substrate-Directed Growth. *Nat. Chem.* **2012**, *4*, 215−220.
(17) Grill, L.; Dyer, M.; Lafferentz, L.; Persson, M.; Peters, M. V.; Hecht, S. Nano-Architectures by Covalent Assembly of Molecular Building Blocks. *Nat. Nanotechnol.* **2007**, *2*, 687−691.
(18) Xia, T. K.; Landman, U. Molecular-Dynamics of Adsorption and Segregation from an Alkane Mixture. *Science* **1993**, *261*, 1310−1312.
(19) Hentschke, R. Molecular Modeling of Adsorption and Ordering at Solid Interfaces. *Macromol. Theory Simul.* **1997**, *6*, 287−316.
(20) Fodi, B.; Hentschke, R. Molecular Dynamics Simulation of a Binary Hydrocarbon Mixture near an Adsorbing Wall: Benzene/n-Heptane on Graphite. *Langmuir* **1998**, *14*, 429−437.
(21) Mali, K. S.; Van Averbeke, B.; Bhinde, T.; Brewer, A. Y.; Arnold, T.; Lazzaroni, R.; Clarke, S. M.; De Feyter, S. To Mix or Not To Mix: 2D Crystallization and Mixing Behavior of Saturated and Unsaturated Aliphatic Primary Amides. *ACS Nano* **2011**, *5*, 9122−9137.
(22) De Cat, I.; Gobbo, C.; Van Averbeke, B.; Lazzaroni, R.; De Feyter, S.; van Esch, J. Controlling the Position of Functional Groups at the Liquid/Solid Interface: Impact of Molecular Symmetry and Chirality. *J. Am. Chem. Soc.* **2011**, *133*, 20942−20950.
(23) Smith, P.; Lynden-Bell, R. M.; Smith, W. The Behaviour of Liquid Alkanes near Interfaces. *Mol. Phys.* **2000**, *98*, 255−260.
(24) Balasubramanian, S.; Klein, M. L.; Siepmann, J. I. Monte-Carlo Investigations of Hexadecane Films on a Metal-Substrate. *J. Chem. Phys.* **1995**, *103*, 3184−3195.
(25) Marrink, S. J.; Risselada, H. J.; Yefimov, S.; Tieleman, D. P.; de Vries, A. H. The MARTINI Force Field: Coarse Grained Model for Biomolecular Simulations. *J. Phys. Chem. B* **2007**, *111*, 7812−7824.
(26) Marrink, S. J.; de Vries, A. H.; Mark, A. E. Coarse Grained Model for Semiquantitative Lipid Simulations. *J. Phys. Chem. B* **2004**, *108*, 750−760.
(27) Wong-Ekkabut, J.; Baoukina, S.; Triampo, W.; Tang, I. M.; Tieleman, D. P.; Monticelli, L. Computer Simulation Study of Fullerene Translocation through Lipid Membranes. *Nat. Nanotechnol.* **2008**, *3*, 363−368.
(28) Wallace, E. J.; Sansom, M. S. P. Blocking of Carbon Nanotube Based Nanoinjectors by Lipids: a Simulation Study. *Nano Lett.* **2008**, *8*, 2751−2756.
(29) Wu, D.; Yang, X. N. Coarse-Grained Molecular Simulation of Self-Assembly for Nonionic Surfactants on Graphene Nanostructures. *J. Phys. Chem. B* **2012**, *116*, 12048−12056.
(30) Baron, R.; Trzesniak, D.; de Vries, A. H.; Elsener, A.; Marrink, S. J.; van Gunsteren, W. F. Comparison of Thermodynamic Properties of Coarse-Grained and Atomic-Level Simulation Models. *ChemPhysChem* **2007**, *8*, 452−461.
(31) Hess, B.; Kutzner, C.; van der Spoel, D.; Lindahl, E. Gromacs 4: Algorithms for Highly Efficient, Load-Balanced, and Scalable Molecular Simulation. *J. Chem. Theory Comput.* **2008**, *4*, 435−447.
(32) Berendsen, H. J. C.; Postma, J. P. M.; Vangunsteren, W. F.; Dinola, A.; Haak, J. R. Molecular-Dynamics With Coupling to an External Bath. *J. Chem. Phys.* **1984**, *81*, 3684−3690.
(33) Fritz, D.; Koschke, K.; Harmandaris, V. A.; van der Vegt, N. F. A.; Kremer, K. Multiscale Modeling of Soft Matter: Scaling of Dynamics. *Phys. Chem. Chem. Phys.* **2011**, *13*, 10412−10420.
(34) Gregg, S. J.; Sing, K. S. W. *Adsorption, Surface Area and Porosity*, 2nd ed.; Academic Press: London, 1982.
(35) Denoyel, R.; Beurroies, I.; Lefevre, B. Thermodynamics of Wetting: information Brought by Microcalorimetry. *J. Petrol. Sci. Eng.* **2004**, *45*, 203−212.
(36) Brunauer, S.; Emmett, P. H.; Teller, E. Adsorption of Gases in Multimolecular Layers. *J. Am. Chem. Soc.* **1938**, *60*, 309−319.
(37) Isirikyan, A.; Kiselev, A. V. Absolute Adsorption Isotherms of Vapors of Nitrogen, Benzene and n-Hexane, and Heats of Adsorption of Benzene and n-Hexane on Graphitized Carbon Blacks. 1. Graphitized Thermal Blacks. *J. Phys. Chem.* **1961**, *65*, 601−607.
(38) Avgul', N. N.; Berezin, G. I.; Kiselev, A. V.; Lygina, I. A. The Adsorption and Heat of Adsorption of Normal Alcohols on Graphitized Carbon Black. *Russ. Chem. Bull.* **1961**, *10*, 186−193.
(39) Findenegg, G. H.; Liphard, M. Adsorption from Solution of Large Alkane and Related Molecules onto Graphitized Carbon. *Carbon* **1987**, *25*, 119−128.
(40) Findenegg, G. H. Order-Disorder Transitions at Liquid/Solid Interface - Volumetric Behavior of Primary Aliphatic Alcohols near Graphon Surface. *J. Chem. Soc., Faraday Trans.* **1972**, *68*, 1799−1806.
(41) Snyder, R. G.; Goh, M. C.; Srivatsavoy, V. J. P.; Strauss, H. L.; Dorset, D. L. Measurement of the Growth-Kinetics of Microdomains in Binary n-Alkane Solid-Solutions by Infrared Spectroscopy. *J. Phys. Chem.* **1992**, *96*, 10008−10019.
(42) Hosier, I. L.; Bassett, D. C. On Permanent Cilia and Segregation In the Crystallization of Binary Blends of Monodisperse n-Alkanes. *Polymer* **2002**, *43*, 307−318.
(43) Hacura, A.; Kaczorowska, B. Analysis of Segregation Process of n-Alkanes in Binary Mixtures by FT-IR and Raman Spectroscopy. *J. Raman Spectrosc.* **2005**, *36*, 1029−1033.
(44) Rabe, J. P.; Buchholz, S. Commensurability and Mobility in 2-Dimensional Molecular-Patterns on Graphite. *Science* **1991**, *253*, 424−427.
(45) Bienvogelsang, U.; Findenegg, G. H. Monolayer Phase-Transitions of Dodecanol at the Liquid Graphite Interface. *Colloids Surf.* **1986**, *21*, 469−481.
(46) Findenegg, G. H. Ordered Layers of Aliphatic Alcohols and Carboxylic-Acids at Pure Liquid-Graphite Interface. *J. Chem. Soc., Faraday Trans.* **1973**, *69*, 1069−1078.
(47) Marrink, S. J.; Risselada, J.; Mark, A. E. Simulation of Gel Phase Formation and Melting in Lipid Bilayers Using a Coarse Grained Model. *Chem. Phys. Lipids* **2005**, *135*, 223−244.
(48) Humphrey, W.; Dalke, A.; Schulten, K. VMD: Visual Molecular Dynamics. *J. Mol. Graph. Model.* **1996**, *14*, 33−38.